JOURNAL OF SPACECRAFT AND ROCKETS
Vol. 32, No. 2, March–April 1995

Autonomous Navigation for Lunar Transfer

Dan G. Tuckness* and Shih-Yih Young†
University of Texas at Arlington, Arlington, Texas 76019-0018

The primary objective of an onboard autonomous navigation sensor is to estimate the states of the spacecraft without the use of ground support and arrive at its destination with a high degree of accuracy. This paper presents a preliminary investigation into the feasibility of an autonomous lunar transfer navigation scheme using discrete onboard angle-only measurements. System observability using the angle-only scheme is formulated and discussed. Two approaches, optimal design and suboptimal design, are investigated. A simulation was performed to compare the two methods. Results of the simulation show that the suboptimal approach offers accuracy close to the optimal approach but requires much less processing.

Nomenclature

A	= matrix describing the relative target-to-observer Nth-order dynamics
A_g	= $N \times N$ state gradient matrix
B	= matrix describing the observer dynamics
F	= $N \times 1$ set of the equations of motion of the spacecraft
G	= $N \times M$ sensor model matrix
G	= universal gravitational constant
$g(t), G(t)$	= observer maneuver
H	= observation measurement matrix
K	= $N \times M$ Kalman-filter gain matrix
N	= number of states
M	= number of measurement sources
P	= $N \times N$ covariance matrix before propagation to measurement processing time
$\bar{P}$	= $N \times N$ covariance matrix after propagation to measurement processing time
$P(-)$	= $N \times N$ covariance matrix before measurement update
$P(+)$	= $N \times N$ covariance matrix after measurement update
Q	= $N \times 1$ state noise matrix
r	= radial distance, m
R	= $1 \times M$ navigation measurement noise matrix
SC	= spacecraft
$s(t)$	= target trajectory
V	= measurement noise
W	= $N \times 1$ state weighting matrix (identity matrix for this study)
$w(t)$	= observer trajectory
X	= $N \times 1$ state vector
Z	= measurement vector
α	= azimuth angle, rad
$\alpha(t)$	= arbitrary scaling function
β	= elevation angle, rad
$\lambda(t)$	= arbitrary scaling function
Φ	= $N \times 1$ state transition matrix

Introduction

GROUND-BASED tracking stations, such as the Deep Space Network (DSN), measure the radial distance between the ground-based tracking-station antenna, SC, and the SC destination in order to compute the relative position of the SC with respect to the earth and its target destination. An onboard autonomous navigation sensor could also measure the radial distance between itself and the earth in order to compute its relative position. This could be done using a SC transmitter and earth-based repeater for ranging, as usual. However, that would require a ground-based repeater or other transmitter. For the SC to be fully autonomous, it must not rely on ground-based navigation aids. In order to measure the range to the earth, or any another celestial body, the SC would be required to transmit a signal strong enough to bounce off the Earth's surface. One of the bigger problems with that approach would be the dispersion and attenuation of the SC transmitted signal when it passes through the Earth's atmosphere. Passage through the atmosphere weakens the SC received signal. Because an SC antenna, such as that used by the DSN to receive weak interplanetary SC signals, may not have sufficient gain, an alternative method of determining the range to the earth warrants investigation.

This paper investigates relieving the requirement of physically measuring SC range by resolving range information through angle-only measurements. Angle measurements of the earth, moon, and sun during a translunar trajectory are processed through an extended Kalman filter (EKF) in order to obtain the range information. The size of the EKF (number of processed states) is also addressed, since most onboard navigation computers are limited in memory and computational power. It will be shown in this paper that sensor accuracy does not appear to be a major problem: today's sensor accuracies should be accurate enough for angle-only navigation. A major area of concern with the angle-only navigation pertains to the observability criteria of the measurement equations. It will be shown that the system unobservability found when using certain types of navigation measurements is a major obstacle in the angle-only navigation scheme but can be overcome if properly addressed.

Navigation Filter Size and Processing

Before the differences between the optimal and suboptimal navigation filters are fully explained, a brief discussion of the EKF used to process the measurements is in order. The EKF estimates the "cloud of uncertainty" (covariance matrix) surrounding the state vector and aids in removing this navigation uncertainty using discrete measurement updates. In this study, the EKF processes the angle-only measurements at 1-h intervals. It is assumed that all the measurements are acquired simultaneously. This can easily be achieved through the use of multiple sensor mountings and processors. A brief mathematical model and flow of the EKF is given below. A more in-depth discussion of the EKF and of optimal and suboptimal filter design is found in Ref. 1.

The time derivative of the state vector and the state transition matrix are calculated using

$$\dot{X} = F(X, t) \tag{1}$$

$$\dot{\Phi} = A_g \Phi \tag{2}$$

Received Sept. 1, 1993; revision received Oct. 12, 1994; accepted for publication Oct. 30, 1994.

*Assistant Professor, Department of Mechanical and Aerospace Engineering, Box 18018. Member AIAA.

†Research Assistant, Department of Mechanical and Aerospace Engineering, Box 18018.

The covariance matrix of the state variables is propagated up to the time of measurement using

$$P(-) = \Phi \bar{P}(-)\Phi^T + Q \tag{3}$$

where Q is a white sequence of random noise with zero mean. This assumes there is an a priori covariance matrix; it is given later in this paper.

The observation update matrix is computed using the current state vector:

$$H = \frac{\partial G(X, t)}{\partial X} \tag{4}$$

The estimated measurement values are then calculated using

$$Z = HX + V \tag{5}$$

where V is white Gaussian noise with zero mean and covariance R.

The Kalman filter gain equation is used to compute the Kalman gain:

$$K = P(-)H^T[HP(-)H^T + R]^{-1} \tag{6}$$

The covariance matrix is then updated to include the effects of the measurement using

$$P(+) = (I - WKH)P(-)(I - WKH)^T + WKRK^T \tag{7}$$

The best estimate is then calculated using

$$\hat{X} = X + KZ \tag{8}$$

Now, set, $\bar{P}(-) = P(+)$ and $X = \hat{X}$ for the next measurement processing and/or iteration.

Optimal EKF Filter Design

Basically, an optimal filter must model all error sources in the system at hand. It is assumed in the filter equations that exact descriptions of the system dynamics, error statistics, and measurement processes are known. Therefore, the optimal filter processes all the states that influence the equations of motion of the SC through the EKF. The equations of motion of the SC are dominated by the effects of the sun, earth, and moon. Therefore, it is necessary to estimate (process) the states of the sun, earth, and moon in order to determine the states of the SC. The overall system is four-body motion, resulting in 18 states being processed through the EKF ($N = 18$). Therefore, propagation of the covariance matrix using Eq. (3) requires the multiplication of three matrices of size 18×18. This requires 972 multiplication operations (including redundant multiplication for symmetric terms), which results in the expenditure of large amounts of computation time.

Suboptimal EKF Filter Design

Most onboard navigation computers have limited computing capabilities and speed. Therefore, it is desirable to develop a navigation filter algorithm that results in the smallest processing memory and storage space possible. Reduction of computation requirements is addressed two ways. First, the suboptimal filter is not required to numerically integrate the full equations of motion. Instead, it uses a table lookup of the earth and moon ephemerides data to determine their dynamical positions. Second, because it can be time-consuming to process 18 states through the EKF, a suboptimal filter that processes only the states of the SC is implemented. This makes the EKF "blind" to the motion of the sun and moon resulting in a suboptimal filter. The total number of estimated states in the suboptimal filter is six (the states of the SC), and propagation of the covariance matrix now requires the multiplication of three matrices of size 6×6. This is only 11% of the multiplications required for the optimal design.

Observability of the System

Dynamical Conditions for Observability

An important consideration in estimating a target trajectory using external sensor measurements is defining the target observability criteria, i.e., the necessary and sufficient conditions to ensure a unique estimate of the target trajectory given a finite set of noise-corrupted observations (measurements). In radar tracking systems, where range and angular positions with respect to the radar antenna are acquired, each measurement vector determines the instantaneous target position within a finite uncertainty volume. Therefore, uncertainties in both range and angles are expressed with finite standard deviations, and a unique minimum-variance estimate is obtained. In an angle-only tracking system, the uncertainty volume of each (sun, earth, and moon) positional measurement vector is infinite (due to the inability to measure range), and the system will be unobservable. However, when the order of the observer (the SC in this study) dynamics is least one higher than the order of the target (moon) dynamics, the system is observable. This is shown by letting the target and the observer trajectories be represented by three-dimensional Cartesian vectorial functions $s(t)$ and $w(t)$, respectively. It is assumed that the function $w(t)$ is known and $s(t)$ is to be estimated using SC-to-target measurements. Let

$$u(t) = r(t)/\|r(t)\| \tag{9}$$

where $r(t) = s(t) - w(t)$, and $\|r(t)\|$ denotes the norm of the vector $r(t)$. Modeling the target motion by Nth-order dynamics

$$s(t) = At \tag{10}$$

(where $t = [1\ 1\ t\ t^2\ \cdots\ t^N]^T$ and A is a $3 \times (N+1)$ matrix of target-trajectory undetermined coefficients that are to be estimated), the observer's trajectory is defined as

$$w(t) = Bt - g(t) \tag{11}$$

Here B is the $3 \times (N+1)$ matrix describing the observers Nth-order dynamics, and $g(t) = [g_1(t), g_2(t), g_3(t)]^T$ represents the observer's maneuver. The importance of the equation for $g(t)$ is that it does not contain powers of t less than $N+1$. Subtracting Eq. (11) from Eq. (10) gives

$$r(t) = Rt + g(t) \tag{12}$$

where $R = A - B$ and estimating r is equivalent to estimating the trajectory. From Eq. (9), $r(t) = \|r(t)\|u(t)$, and representing $\|r(t)\|$ as a scalar function $\lambda(t)$ gives

$$r(t) = \lambda(t)u(t) \tag{13}$$

Combining Eqs. (12) and (13) yields

$$Rt + g(t) = \lambda(t)u(t) \tag{14}$$

In order to derive the uniqueness condition required for the solution for R, assume there exist two distinct solutions R_1 and R_2, associated with scalar functions $\lambda_1(t)$ and $\lambda_2(t)$, respectively. Substituting both solutions into Eq. (14) and subtracting gives

$$[\lambda_1(t) - \lambda_2(t)]u(t) = (R_1 - R_2)t \tag{15}$$

Thus, the solution of Eq. (14) is unique if, and only if, there exist no two distinct matrices R_1 and R_2 satisfying Eq. (15). Finally, from Eqs. (13) and (15) ,the necessary and sufficient conditions for three-dimensional, Nth-order dynamic observability are obtained:

$$r(t) \neq \alpha(t)At \tag{16}$$

where $\alpha(t)$ is an arbitrary scalar function and A is a $3 \times (N+1)$ matrix of system coefficients. Therefore, the SC motion $r(t)$ must be

at least one order higher than the system (At). This means that the SC must undergo jerk (time derivative of acceleration) in order to be one order higher than the planetary acceleration (system) acting on the SC. A more in-depth discussion of maneuver-induced observability is found in Refs. 2 through 4.

Note that other external forces acting on the SC, such as solar radiation forces, could result in weak observability but are reserved for future studies in order to concentrate on the dominant external forces. Also, note that if there is continuous thrust applied to the SC during the lunar transfer (as on a low-thrust mission), the system is observable.

The preceding proof is for a set of solved equations of motion where the position and velocity of the SC are described through a set of time-variant polynomials. However, for the system under consideration in this study (three or more bodies), no closed-form solution exists. Therefore, the equations of motion must be integrated numerically in order to obtain the positions and velocities. The approach used above in proving observability of two bodies can be used in proving observability for the three or more bodies without solving the equations of motion explicitly as a function of time.

Given the equations of motion of the observer (SC) as

$$\ddot{\boldsymbol{X}}_1 = \boldsymbol{f}(\boldsymbol{X}_1, \boldsymbol{X}_2) - \boldsymbol{g}(t) \tag{17}$$

and for the target (moon) as

$$\ddot{\boldsymbol{X}}_2 = \boldsymbol{h}(\boldsymbol{X}_1, \boldsymbol{X}_2) \tag{18}$$

where $\boldsymbol{g}(t)$ is an external force such as thrust, their positions can be represented as

$$\boldsymbol{X}_1(t) = \iint \boldsymbol{f}(\boldsymbol{X}_{10}, \boldsymbol{X}_{20}, t)\, \mathrm{d}t\, \mathrm{d}t - \iint g(t)\, \mathrm{d}t\, \mathrm{d}t \tag{19}$$

$$\boldsymbol{X}_2(t) = \iint \boldsymbol{h}(\boldsymbol{X}_{10}, \boldsymbol{X}_{20}, t)\, \mathrm{d}t\, \mathrm{d}t \tag{20}$$

where $\boldsymbol{X}_{10}, \boldsymbol{X}_{20}$ are the initial position vectors of the observer and target respectively. Equations (19) and (20) can be rewritten as

$$\boldsymbol{X}_1(t) = \boldsymbol{u}(\boldsymbol{X}_{10}, \boldsymbol{X}_{20}, t) - \boldsymbol{G}(t) \tag{21}$$

$$\boldsymbol{X}_2(t) = \boldsymbol{s}(\boldsymbol{X}_{10}, \boldsymbol{X}_{20}, t) \tag{22}$$

Now

$$\begin{aligned} \boldsymbol{r}(t) &= \boldsymbol{X}_2(t) - \boldsymbol{X}_1(t) \\ &= \boldsymbol{s}(\boldsymbol{X}_{10}, \boldsymbol{X}_{20}, t) - \boldsymbol{u}(\boldsymbol{X}_{10}, \boldsymbol{X}_{20}, t) + \boldsymbol{G}(t) \end{aligned} \tag{23}$$

Rewrite Eq. (23) as

$$\boldsymbol{r}(t) = \boldsymbol{R}(\boldsymbol{X}_{10}, \boldsymbol{X}_{20}, t) + \boldsymbol{G}(t) \tag{24}$$

By using two angular components, $\boldsymbol{u}(t) = \boldsymbol{f}(\alpha, \beta), \boldsymbol{r}(t)$ can be written as

$$\begin{aligned} \boldsymbol{r}(t) &= \boldsymbol{R}(\boldsymbol{X}_{10}, \boldsymbol{X}_{20}, t) + \boldsymbol{G}(t) \\ &= \lambda(t)\boldsymbol{u}(t) \end{aligned} \tag{25}$$

Assume two distinct solutions $\boldsymbol{R}_1$ and $\boldsymbol{R}_2$ are associated with the scalar functions $\lambda_1(t)$ and $\lambda_2(t)$, respectively. Substituting both solutions into Eq. (25) and subracting the results yields

$$[\lambda_1(t) - \lambda_2(t)]\boldsymbol{u}(t) = \boldsymbol{R}_1(\boldsymbol{X}_{10}, \boldsymbol{X}_{20}, t) - \boldsymbol{R}_2(\boldsymbol{X}_{10}, \boldsymbol{X}_{20}, t) \tag{26}$$

Thus, the solution of Eq. (25) is unique if, and only if, there exist no two distinct matrices $\boldsymbol{R}_1$ and $\boldsymbol{R}_2$ satisfying Eq. (26). Therefore, the necessary and sufficient condition for this case is

$$\boldsymbol{r}(t) \neq \alpha(t)\boldsymbol{B}(\boldsymbol{X}_{10}, \boldsymbol{X}_{20}, t) \tag{27}$$

where $\alpha(t)$ is an arbitrary scalar function and $\boldsymbol{B}$ is the matrix describing the observer dynamics. Therefore, the observer relative distance to the target, $\boldsymbol{r}(t)$, cannot be only a function of the system state, and the observer must have an external force acting on it in order to be observable.

Looking at Eq. (25) shows that

$$\boldsymbol{r}(t) = \boldsymbol{R}(\boldsymbol{X}_{10}, \boldsymbol{X}_{20}, t) + \boldsymbol{G}(t) \tag{28}$$

which includes the additional maneuvering term $\boldsymbol{G}(t)$ and is the key ingredient in making the system observable.

Both proofs above express the fact that if no external forces are being applied to the SC during the navigation processing (as when navigation is taking place between the ΔV burns, which happens to be the case during most of the translunar trajectory), the order of the dynamics of the destination target is the same as that of the observer (SC), making the system *translational motion* unobservable. Therefore, according to Eq. (16) and Eq. (17), angle-only navigation can only take place when the SC is thrusting or some other external force is acting on the SC. However, these two equations rely only on the dynamics of the system. It will be shown in the next section that if one looks at the case of observability from a geometric perspective, full observability can be obtained without thrusting, making angle-only navigation feasible.

Geometric Observability of a System Using Angle-Only Measurements

The angles measured using the angle-only navigation method are the azimuth and elevation angles of the sun, earth, and moon with respect to the SC flight-path axis shown in Fig. 1. The actual angular measurements, sensor accuracies, etc., will be discussed later in this paper and for now are assumed achievable. By observing the azimuth and elevation angles of the sun, earth, and moon, the unit vectors along the lines of sight to the sun, earth, and moon can be obtained. Because of the pointing inaccuracies of the sensors, the uncertainty volumes of the relative distances will be shaped like cones whose sizes are a function of the sensor's inaccuracies . By using at least two or more nonparallel unit vectors, the cones will intersect each other. The intersected volume is finite, and the true SC states will be contained within this finite volume. From this, the states of the earth, sun, and moon are now known to within a finite value. Therefore, they are represented as a standard deviation of error with respect to the unknown true states. Although the exact position of the observer with respect to the target is not known, the uncertainty in the position is now finite (bounded). Using estimation theory, this finite region of error can be resolved through the process of taking measurements and reducing the uncertainty of its size. This is done by reducing the covariance matrix by processing the angle-only measurements through the EKF. Thus the positions of the SC are estimated using angle-only measurements, making the system observable.

Numerical Analysis

Description of Coordinate Systems

The coordinate systems used in this analysis are defined according to AIAA standards and are shown in Fig. 1. The SC flight-path coordinate system (x_k, y_k, z_k) is AIAA Standard 1.1.10, and the inertial coordinate system (X_I, Y_I, Z_I) is AIAA Standard 1.1.1.[5] Both

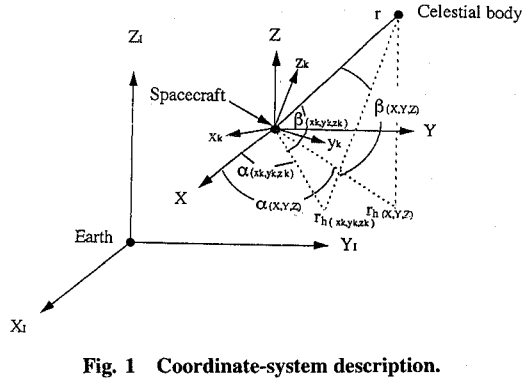

Fig. 1 Coordinate-system description.

Table 1 Definitions of spacecraft flight path and inertial frame coordinates

Axis	Spacecraft flight path: (x_k, y_k, z_k) coordinates	Inertial frame: (X, Y, Z) coordinates
X	Spacecraft velocity	Vernal equinox
Y	(Spacecraft radial range from earth) × (spacecraft velocity)	(Z direction) × (X direction)
Z	(X direction) × (Y direction)	Direction of the north pole (⊥ earth equatorial plane)

Table 2 Initial inertial "true" state vector of spacecraft, sun, moon

	Spacecraft	Sun	Moon
X position, km	−2472.594783	−149147372.9	391195.3
Y position, km	−5502.242178	18025379.68	−5840.91
Z position, km	−2585.802248	7341372.234	35719.82
X velocity, km/s	10.20483337	−3.404645627	−0.07171394
Y velocity, km/s	−3.861811468	−26.99479627	0.9162825
Z velocity, km/s	−0.581308402	−11.7048515	0.3841142

Table 3 Sensor biases and noises (1σ)

Sensor	Sensor bias, deg: Sun	Earth	Moon	Sensor noise for all sensors, deg
A	0.01	0.01	0.01	0.01
B	0.0001	0.0001	0.0001	0.0001

coordinate systems utilize earth-centered (X_I, Y_I, Z_I) inertial calculations. The on-board sensor readouts are easily transformed from the (X_I, Y_I, Z_I) coordinates to the (x_k, y_k, z_k) coordinate system (a coordinate system normally used in performing navigation measurements) or to a coordinate system (X, Y, Z) for the SC gimbaled inertial navigation platform. For navigation performance comparison, angle measurements referenced to the (X, Y, Z) coordinate system are investigated and compared with the measurements referenced to a (x_k, y_k, z_k). Coordinate-system labeling for Fig. 1 is given in Table 1.

Equation of Motion and Numerical Integration

The following is a description of the system, equations of motion, and location of the the SC, sun, and moon in the Cartesian coordinate system. We have

$$\ddot{\boldsymbol{r}} = -\frac{G(m_1 + m_2)\boldsymbol{r}}{r^3} - G\sum_{j=3}^{L} m_j\left(\frac{\boldsymbol{\delta}_j}{\delta_j^3} - \frac{\boldsymbol{\rho}_j}{\rho_j^3}\right) \tag{29}$$

where G is the universal gravitational constant, m_1 is the primary mass (earth) and m_2 is the secondary mass (SC). The directions of $\boldsymbol{r}$, $\boldsymbol{\rho}_j$, and $\boldsymbol{\delta}_j$ are from m_1 toward m_2, from m_1 toward m_j, and from m_2 toward m_j, respectively.

Integration of the equations of motion and covariance matrix is performed using a fourth-order Runge–Kutta integrator with a fixed step size of 10 s. The initial conditions for the states of the sun, moon, and SC are given in Table 2 and are adopted from Refs. 6 through 8. All initial conditions are specified in the J2000 geocentric-equatorial coordinate system.[6]

Sensor Measurements, Models, and Errors

Two sets of angular measurements, the azimuth α and elevation β, of the target with respect to the SC flight-path axis and the SC gimbaled inertial-navigation-system platform frame are shown in Fig. 1. Also, two different types of sensors are examined: A is an off-the-shelf sensor[9]; B is arbitrarily chosen for comparison and has the accuracy of most star trackers, thus being more accurate than sensor A.

Table 3 gives a description of the errors for both sensors.

Table 4 Diagonals of initial covariance matrices of spacecraft, sun, moon

	Spacecraft	Sun	Moon
X position, km^2	4.0	25,000,000	250,000
Y position, km^2	4.0	25,000,000	250,000
Z position, km^2	4.0	25,000,000	250,000
X velocity, km/s^2	0.01	2.25	0.25
Y velocity, km/s^2	0.01	2.25	0.25
Z velocity, km/s^2	0.01	2.25	0.25

Navigation Filter Model Initial Conditions

The differences between the initial estimates [initial best estimate $(\hat{\boldsymbol{x}})$] and initial truth states given in Table 2 are 2.0, 5000.0, and 500.0 km for the (X, Y, Z) positions, and 0.1, 1.5, and 0.5 km/s for the (X, Y, Z) velocities, for the SC, sun, and moon, respectively. These errors were obtained from Ref. 7. The off-diagonal terms of the initial covariance matrix are all zero, and the diagonal terms are given in Table 4.

Ephemeris Error for Use of Ephemeris Table Lookup

It is highly probable that the ephemerides of the sun and moon used in the suboptimal study are more accurate than the nonlinear equations of motion used in the optimal study. Therefore, the initial errors in the state of the sun and moon for the suboptimal case will be smaller than those used in the optimal study. Because the ephemerides contain uncertainties in the location of the centers of mass of the sun and moon, white Gaussian noise is added to approximate the error in the ephemeris data. The amount of error is adopted from Ref. 7, and the systematic differences between planetary observations and ephemeris are also discussed in that reference. According to Ref. 7, the differences between the sun observations and the ephemeris is less than 2″ (about 3000 km) and is dependent on the season. A conservative 5000-km uncertainty in the ephemeris of the sun is adopted for this investigation.

The distance between the surface of the moon and the surface of the earth has been measured to centimeter accuracy, but not the distance between the center of mass of the moon and the center of mass of the earth. Therefore, 10 km is assumed for the uncertainty of the ephemeris of the moon for this investigation.

Navigation Filtering Assumptions

The numerical investigation addresses the errors due to the sensor pointing inaccuracies and the uncertainty in the a priori covariance matrix. By assuming that there is no system noise in this simulation, the equations of motion of the sun, moon, and SC are completely known. Therefore, the estimates processed through the EKF should approach the true states. The system noise is assumed zero in order to aid in understanding the problems at hand. Inclusion of system noise allows for a Bayesian estimation and in many circumstances results in better filter performance. The reader is directed to Ref. 1 for a more detailed explanation.

Again, to concentrate on the influence of sensor pointing inaccuracies and the uncertainty in the a priori covariance matrix, the effects of the Jupiter and Saturn are not included in this preliminary investigation. These effects are treated as system noises, since the influence of these planets over the short duration of the lunar transfer is minimal.

For this study the distance between the moon and SC is chosen as the performance measure, because of its importance in an earth-to-moon transfer.

Results of Numerical Navigation Analysis

No Measurement Updates

For comparison, Fig. 2 shows the moon root mean square (rms) distance error (difference between the estimated moon distance and the true moon distance) verses transfer time for the case without navigation updates. As expected, there is a large divergence between

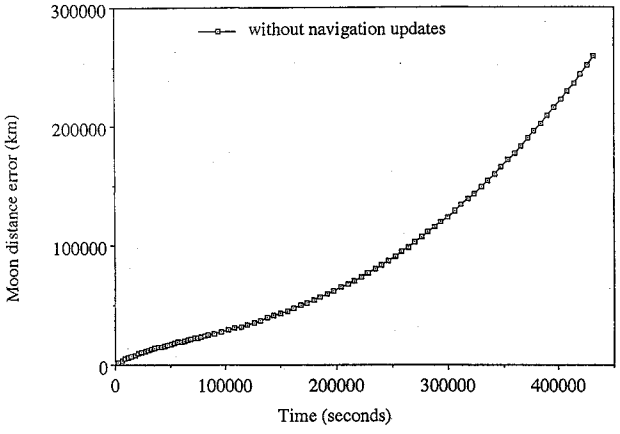

Fig. 2 Moon distance error for lunar transfer without navigation update.

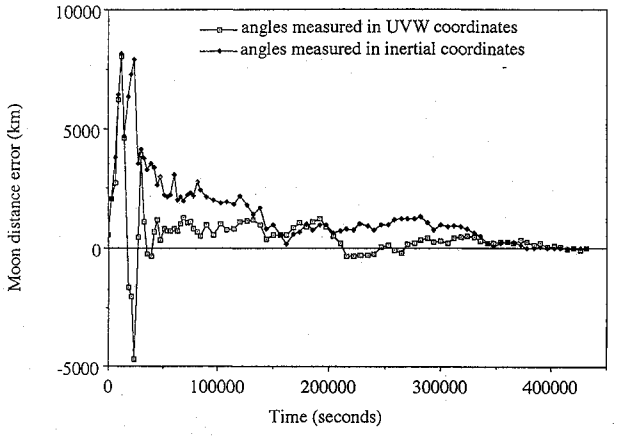

Fig. 3 Optimal design for Cartesian coordinates.

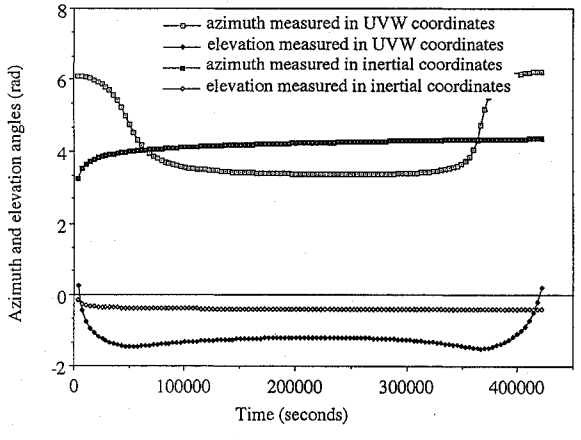

Fig. 4 Earth angles (azimuth and elevation) measured in two different coordinate systems.

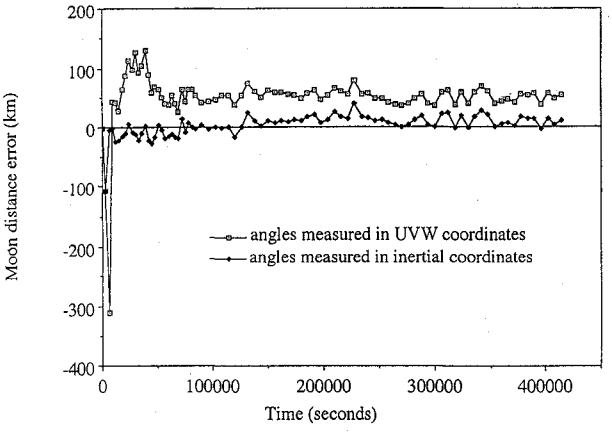

Fig. 5 Suboptimal design for Cartesian coordinates.

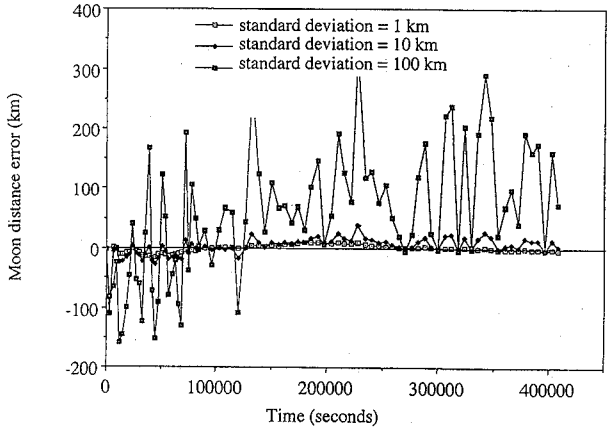

Fig. 6 Suboptimal design with three different standard deviations of the noise of the ephemeris of the moon.

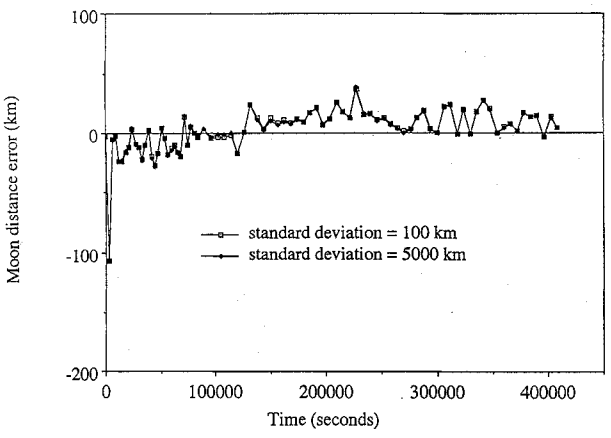

Fig. 7 Suboptimal design with two different standard deviations of the noise of the ephemeris of the sun.

the estimated moon distance and true moon distance after the 5-day lunar transfer time period.

Optimal Design

Figure 3 presents the rms moon distance error versus transfer time, utilizing angular measurements, for the two coordinate systems investigated (flight path and inertial). It can be seen that the EKF has smaller initial oscillation (i.e., smaller initial changes in the covariance) and converges closer to the true states with angles measured in SC flight-path coordinates than, with angles measured in the inertial frame. The reason is that angles change more rapidly in the flight-path coordinates. Figure 4 depicts the azimuth and elevation angles of the earth with respect to the SC versus transfer time. Observing Fig. 4, one can see that the rates of change of the azimuth and elevation are greater in the SC flight-path coordinate system than in the inertial coordinate system, thus increasing the degree of observability. The rms moon distance error after the 5-day lunar transfer time is about 3 km. Therefore, the states of the SC and moon can be estimated with reasonable accuracy without any ground support.

Suboptimal Design

Figure 5 depicts the moon distance error versus lunar transfer time. The standard deviation of the noise for the ephemeris of the sun is 5000 km, and the standard deviation of the noise for the ephemeris

Table 5 Rms moon distance errors at moon arrival for Figs. 2 through 8

	Fig. 2, km	Fig. 3, km	Fig. 4, rad	Fig. 5, km	Fig. 6, km	Fig. 7, km	Fig. 8 Optimal design, km	Fig. 8 Suboptimal design, km
No update	2.44E5							
$x_k, y_k, z_k\ \alpha$			6.20					
$x_k, y_k, z_k\ \beta$			1.81					
Inertial α			4.34					
Inertial β			−0.41					
Diag				2.90				
Couple				6.42				
Inertial		10.1						
x_k, y_k, z_k		2.9						
1 km					−2.79			
10 km					3.90			
100 km					7.20	4.12		
5000 km						3.90		
Sensor A							2.90	18.40
Sensor B							−0.69	2.15

of the moon is 10 km along both angular planes measured in the SC flight-path and inertial coordinate systems. Figure 5 shows that the EKF converges closer to the true states with angles measured in SC flight-path coordinates than with angles measured in the inertial frame. The rms moon distance error after the 5-day lunar transfer is about 10 km. This is only 7 km greater than for the optimal design and required much less processing. In Fig. 6, the standard deviation of the noise for the ephemeris of the sun is 5000 km, and the standard deviations of the noises for the ephemeris of the moon were selected to be 1, 10, and 100 km. As expected, better results can be obtained for smaller standard deviation of the noise for the ephemeris of the moon. In Fig. 7, the standard deviation of the noise for the ephemeris of the moon is 10 km and the standard deviations of the noise for the ephemeris of the sun were selected to be 5000 and 100 km. Figure 7 depicts that the magnitude of the noise from the ephemeris of the sun has very little influence on the performance of EKF. This is because the gravity of the sun is a secondary perturbing force. Also, the angular sun measurement changes very little during the 5-day transfer period. This results in a small influence of the sun measurements and/or noise inputs to the estimation filter.

Sensor Accuracy Effects

Figure 8 shows the moon distance error for the optimal design case when using the EKF system with angular measurements in the SC flight-path coordinate using sensors A and B. As expected, use of better sensors results in faster convergence to the true states. Figure 8 also shows the moon distance error for the suboptimal design case with angular measurements in the SC flight-path coordinate system using sensors A and B. The difference in sensor accuracy between sensor A and sensor B in the suboptimal case is not as great as the difference in the optimal case. Therefore, sensor effect appears to be a secondary factor (secondary to ephemeris error) for the suboptimal design.

Table 5 gives the numerical values for the lunar arrival errors for all cases investigated.

Conclusion

An onboard autonomous navigation scheme is proposed in this paper that uses an EKF with updates from discrete angle measurements. Both the optimal filter design (estimation of all states influencing the equations of motion of the SC) and the suboptimal filter design (estimation of SC states only) show that the moon distance is estimated with fairly good accuracy when using onboard sensors without the aid of ground support. Because the SC will no longer require constant ground support, it is free of ground-support errors such as power outages. On comparing the results between the optimal and suboptimal cases, the authors believe that the suboptimal design is more suitable for actual space missions with regard to navigation filter stability (small stabilization time requirements)

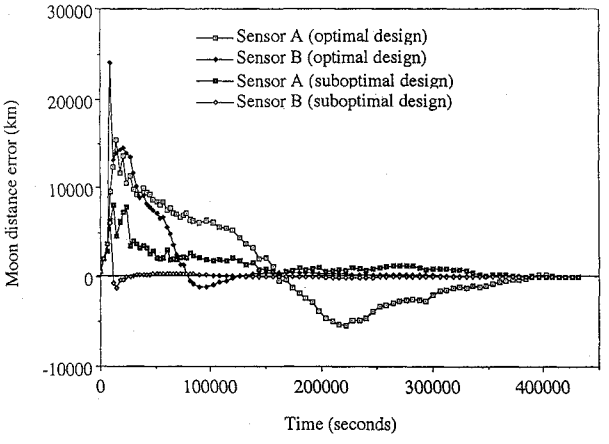

Fig. 8 Optimal and suboptimal design for two different sensors.

and required computational loads (estimating SC states only). Using the suboptimal filter results in a lunar arrival error that is within approximately 10 km of the error found when using the optimal filter. This shows that there is very little difference in performance between the two filters. However, the suboptimal filter requires much less onboard computer calculation and memory, since it only estimates six states instead of the full 18 of the optimal case, making the suboptimal filter much more attractive for onboard navigation.

Areas of concern and current investigations to be addressed in future publications include the following:

1) The planetary geometry and its effect on the observability need additional investigation.

2) The effects of each of the three sensors (sun, earth, and moon) should be investigated independently in order to assess which sensor has the most influence on the performance of the filter.

Acknowledgments

The authors are grateful to the State of Texas, which supported this research under the Advanced Technology Program, Grant 003656089.

References

[1]Gelb, A., *Applied Optimal Control*, MIT Press, Cambridge, MA, 1974.

[2]Fogel, E., and Gavish, M., "*N*th-Order Dynamics Target Observability from Angle Measurements," *IEEE Transactions on Aerospace and Electronic Systems*, Vol. 24, No. 3, 1988, pp. 305–308.

[3]Gorecki, F. D., "Angle-Only-Track, Observability and Information Theory," AIAA Paper 89-3539-CP, Aug. 1989.

[4]Chang, C. B., and Tabaczynski, J. A., "Application of State Estimation to Target Tracking," *IEEE Transactions on Automatic Control*, Vol. AC-29, No. 2, 1984. pp. 98–109.

[5]Anon., "Recommended Practice for Atmospheric and Space Flight Vehicle Coordinate Systems," ANSI/AIAA R-004-1992, Feb. 1992.

[6]Anon., *Planetary and Lunar Coordinates*, H. M. Nautical Almanac Office, Royal Greenwich Observatory, and The Nautical Almanac Office, United States Naval Observatory, 1983.

[7]Seidelmann, P. K., Santoro, E. J., and Pulkkinen, K. F., "Systematic Differences Between Planetary Observations and Ephemerides," *Dynamical Astronomy—Proceedings of the Second U. S. Hungary Workshop*, 1st ed., Univ. of Texas Press, Sept. 1985, pp. 55–65.

[8]Kovalevsky, J., "Modern Lunar Theory," *Applications of Modern Dynamics to Celestial Mechanics and Astrodynamics—Proceedings of the NATO Advanced Study Institute held at Cortina D'Ampezzo* (Aug. 2–14, 1981), D. Reidel, 1981.

[9]Tai, F., and Noerdlinger, P. D., "A Low Cost Autonomous Navigation System," American Astronomical Society, Paper 89-001, Feb. 1989.

A. L. Vampola
Associate Editor